Original Article

Targeted Liquid Biopsy Using Irradiation to Facilitate the Release of Cell-Free DNA from a Spatially Aimed Tumor Tissue

Jae Myoung Noh[1], **Yeon Jeong Kim**[2], **Ho Yun Lee**[3], **Changhoon Choi**[1], **Won-Gyun Ahn**[1], **Taeseob Lee**[2,4], **Hongryull Pyo**[1], **Jee Hyun Park**[1], **Donghyun Park**[2,4], **Woong-Yang Park**[2,5]

[1]Department of Radiation Oncology, Samsung Medical Center, Sungkyunkwan University School of Medicine, Seoul, [2]Samsung Genome Institute, Samsung Medical Center, Seoul, [3]Department of Radiology and Center for Imaging Science, Sungkyunkwan University School of Medicine, Seoul, [4]GENINUS Inc., Seoul, [5]Department of Molecular Cell Biology, Sungkyunkwan University School of Medicine, Suwon, Korea

Purpose We investigated the feasibility of using an anatomically localized, target-enriched liquid biopsy (TLB) in mouse models of lung cancer.

Materials and Methods After irradiating xenograft mouse with human lung cancer cell lines, H1299 (NRAS proto-oncogene, GTPase [*NRAS*] Q61K) and HCC827 (epidermal growth factor receptor [*EGFR*] E746-750del), circulating (cell-free) tumor DNA (ctDNA) levels were monitored with quantitative polymerase chain reaction on human long interspersed nuclear element-1 and cell line-specific mutations. We checked dose-dependency at 6, 12, or 18 Gy to each tumor-bearing mouse leg using 6-MV photon beams. We also analyzed ctDNA of lung cancer patients by LiquidSCAN, a targeted deep sequencing to validated the clinical performances of TLB method.

Results Irradiation could enhance the detection sensitivity of NRAS Q61K in the plasma sample of H1299-xenograft mouse to 4.5-fold. While cell-free DNA (cfDNA) level was not changed at 6 Gy, ctDNA level was increased upon irradiation. Using double-xenograft mouse with H1299 and HCC827, ctDNA polymerase chain reaction analysis with local irradiation in each region could specify mutation type matched to transplanted cell types, proposing an anatomically localized, TLB. Furthermore, when we performed targeted deep sequencing of cfDNA to monitor ctDNA level in 11 patients with lung cancer who underwent radiotherapy, the average ctDNA level was increased within a week after the start of radiotherapy.

Conclusion TLB using irradiation could temporarily amplify ctDNA release in xenograft mouse and lung cancer patients, which enables us to develop theragnostic method for cancer patients with accurate ctDNA detection.

Key words Radiotherapy, Cell-free DNA, Liquid biopsy, Lung neoplasms

Introduction

Tumors are spatially heterogenous and temporally dynamic, with differently evolving genetic clones responsible for disease progression over time. Next-generation sequencing technology can capture intratumor genomic heterogeneity through deep-sequencing of multiple biopsies taken at different times and regions. Characterizing complex intratumor heterogeneity has yielded important insights for therapeutic target selection and drug development. However, characterizing intratumor heterogeneity at a sufficient resolution remains difficult, primarily because of the high risk caused by multiple and repetitive biopsies.

Recently, analyzing circulating (cell-free) tumor DNA (ctD-NA) has been recognized as a powerful, real-time approach to comprehensive genetic profiling of temporally dynamic diseases. Because it removes the need for repeated invasive procedures [1,2], ctDNA has become a promising biomarker for the noninvasive assessment of tumor burden, therapeutic response, and disease progression in cancer patients [3,4]. Moreover, a single-lesion biopsy does not represent intratumor genomic heterogeneity, but a ctDNA analysis contains integrated genetic information from multiple regions because ctDNA in the bloodstream is derived from tumor cells in different regions. Thus, ctDNA analyses have a clear advantage in overcoming tumor heterogeneity, especially for diagnostic purposes. However, a ctDNA analysis cannot identify the tissue-of-origin or characterize the spatial heterogeneity of

tumors. Therefore, ctDNA analyses should continue to be developed, with a focus on addressing those shortcomings.

There is unfortunately no practical way to control or modulate the release of cell-free DNA (cfDNA) in a region of interest, but its release from normal cells and tumor cells into blood is at least partly understood. Because cfDNA is known to be released upon cell death via apoptosis or necrosis, we hypothesized that the induction of tumor cell death in an anatomically defined region would facilitate ctDNA release and thus enable a liquid biopsy enriched with ctDNA released from the target region. To test that hypothesis, we used radiotherapy (RT) as a modality to induce tumor cell death because RT can be delivered to a well-defined anatomical target region. From the perspective of radiation oncology, personalized radiotherapeutic approaches based on biomarkers are now under development, and ctDNA could be a biomarker for radiation response, the detection of minimal/molecular residual disease (MRD), and the early detection of tumor recurrence [5-8].

In this study, we investigated whether RT could enhance the detection sensitivity of ctDNA in mouse models of lung cancer, and we determined the feasibility of anatomically localized, target-enriched liquid biopsy (TLB) using a double-xenograft mouse model. In addition, we evaluated cancer tissue transcripts from animal models to find changes in the cell composition of the tumor microenvironment that we hoped would allow us to discover the mechanism by which ctDNA release was modulated. Furthermore, increases in ctDNA levels were examined in longitudinal plasma samples from lung cancer patients before, during, and after RT.

Materials and Methods

1. Animals and cell culture

BALB/c mice (male, 5-6 weeks old) were purchased from Orient Bio (Seongnam, Korea).

Four types of human non–small cell lung cancer (NSCLC) cell lines, H460, H1299 (Ras mutant), H1975, and HCC827 (epidermal growth factor receptor [EGFR] mutant), were obtained from ATCC (Manassas, VA). All cell lines were cultured with RPMI (Gibco, Carlsbad, CA) or Dulbecco's modified Eagle's medium (Gibco) containing 10% fetal bovine serum and 1% antibiotic-antimycotic (Thermo Fisher Scientific, Waltham, MA) and incubated at 37°C in 5% CO_2.

2. NSCLC xenograft tumor model and irradiation

NSCLC cells, 1×10^6 cells in a 100 μL suspension of Matrigel Basement Membrane Matrix (Corning, Tewksbury, MA), were subcutaneously injected into the hind legs of mice. The double-xenograft model used H1299, H1975, and HCC827

cells. Different mutant types of cancer cells were inoculated into the hind legs of each mouse. Tumor volumes were measured with calipers every 3 days and calculated according to the following formula: volume=$D_{Short}^2 \times D_{Long}/2$. In both the single and two-tumor models, irradiation was delivered to the tumor-bearing legs of the mice in the irradiation groups using 6-MV photon beams from a linear accelerator (Varian Medical System, Palo Alto, CA) when the tumor volume reached 500 mm³ or 1,000 mm³. During irradiation, the mice were anesthetized by an intraperitoneal injection of tiletamine+zolazepam (50 mg/kg) and xylazine (10 mg/kg), under the approval of the Ministry of Food and Drug Safety. At certain times after irradiation, we sacrificed the mice and harvested their plasma and tumor tissues.

3. Immunohistochemistry

Immunohistochemistry (formalin-fixed paraffin-embedded sections) analysis of tumor tissues sections labeling F4/80 at 1/50 dilution (BM8, eBioscience, San Diego, CA). Heat mediated antigen retrieval citrate buffer. Anti-rat IgG, horseradish peroxidase conjugated (Dako, Glostrup, Denmark) was used as the secondary antibody. Hematoxylin was used as a counterstain.

4. Nucleic acid extraction and quantification

Circulating DNA was extracted from plasma using a QIAamp Circulating Nucleic Acid Kit (Qiagen, Santa Clara, CA). Genomic DNA (gDNA) was isolated from blood samples using a QIAamp DNA Mini Kit (Qiagen). An AllPrep DNA/RNA Mini Kit (Qiagen) was used to purify gDNA and mRNA from tissues. DNA/RNA concentrations and purity were quantified using a Nanodrop 8000 UV-Vis spectrometer (Thermo Fisher Scientific) and a Picogreen fluorescence assay on a Qubit 2.0 fluorometer (Life Technologies, Waltham, MA). The fragment size distribution was measured using a 2200 TapeStation Instrument (Agilent Technologies, Santa Clara, CA).

5. Quantification of cfDNA in plasma

To quantify isolated cfDNA, the long interspersed nuclear element-1 (LINE-1) locus was amplified by real-time polymerase chain reaction (PCR) using SYBR Green (Exiqon) according to the manufacturer's protocols. The LINE-1 locus region was amplified by the following pair of PCR primers: hLINE1: 5′-TCA CTC AAA GCC GCT CAA CTA C-3′, 5′-TCT GCC TTC ATT TCG TTA TGT ACC-3′ and mLine1: 5′-GGA GGG ACA TTT CAT TCT CAT CA-3′, 5′-GCT GCT CTT GTA TTT GGA GCA TAG A-3′. The Ct (threshold cycle) values of the target genes were determined using LightCycler 480 software (Roche, Branchburg, NJ).

To validate the mutations in the NSCLC cell lines, drop-

let digital PCR (ddPCR) was performed using a QX200TM Droplet Digital PCR System (Bio-Rad, Hercules, CA) according to the manufacturer's guidelines. The TaqMan ddPCR Liquid Biopsy Assays for NRAS p.Q61K and EGFR p.E746–A750del (Hs000000079_rm and Hs000000027_rm, Life Technologies) were used. The ddPCR data were analyzed using QuantaSoft software (Bio-Rad).

6. Library preparation

Purified gDNA was sonicated (7 minutes, 0.5% duty, intensity of 0.1, and 50 cycles/burst) into 150-200 bp fragments using a Covaris S2 (Covaris Inc., Woburn, MA). The tumor biopsy sample libraries were constructed using a SureSelect XT reagent kit, HSQ (Agilent Technologies) according to the manufacturer's instructions. The peripheral blood lymphocytes and plasma DNA libraries were created using a KAPA Hyper Prep Kit (Kapa Biosystems, Woburn, MA). Briefly, after completing end repair and A-tailing according to the manufacturer's protocol, we performed adaptor ligation at 4°C overnight using a pre-indexed PentAdapter (PentaBase ApS, Soendersoe, Denmark). Hybrid selection was performed using customized baits that targeted ~117 kb of the human genome, including exons from 38 cancer-specific genes (S1 Table). Sequencing libraries for whole exome sequencing were created using the SureSelect XT Human All Exon V5 kit (Agilent Technologies) and subsequently analyzed on a HiSeq 2500 system (Illumina, San Diego, CA) using the 100-bp paired-end mode of the TruSeq Rapid PE Cluster kit and TruSeq Rapid SBS kit (Illumina).

7. Sequencing data processing

All liquid biopsy data were aligned to the hg19 reference using BWA-mem (v0.7.5) and analyzed as previously reported [9]. During processing, discordant pairs and off-target reads were filtered out. Whole transcriptome data for the xenograft mouse model were generated on an Illumina HiSeq 2500 system, and the sequences were aligned to a mixed genome of GRCh37 and GRChm38 by STAR 2.5.2b. Using RSEM 1.3.0, we quantified the aligned sequences into separate mouse and human transcriptomic expression levels and then merged the levels into each gene to calculate the transcripts per million values representing their gene expression. The cell-type deconvolution analysis was performed by MuSiC [10] for the RNA data from each mouse to characterize 5 distinct cell types in the bulk data. We measured the cell-type composition across each sample to compare the proportions of individual cell types.

8. Detection of somatic mutations

First, all bases were subjected to Phred quality filtering using a threshold Q of 30, and only positions where total depths were above 500× were considered for variant identification. The error suppression method using unique molecular identifiers was carried out to select highly confident reads supporting a non-reference. Non-reference alleles present at a frequency greater than 1% in the matched germline DNA were removed. Otherwise, non-reference alleles were subjected to the binomial test to determine if a non-reference allele was significantly more abundant in plasma DNA than the matched germline DNA (Bonferroni adjusted p-value < 0.01). To minimize false-positives due to cross-contamination among multiplexed samples, we also excluded non-reference alleles if they were found as germline single nucleotide polymorphisms in other samples processed in a capture reaction or the same lane of a sequencing flow cell. Variant candidates with a high strand bias (90% if supporting reads ≥ 20; Fisher exact test, p-value < 0.1 if supporting reads < 20) were removed. Next, we performed a Z-test to identify variants that were present at a significantly higher frequency than the corresponding background errors in the normal samples (Bonferroni adjusted p-value < 0.05). We further applied the following threshold as previously reported [9]. Variants that passed the filter in Strelka2 were further considered.

9. Statistical analysis

All statistical data were analyzed using GraphPad Prism (GraphPad Software, La Jolla, CA). All data were evaluated using analysis of variance (ANOVA) with the Bonferroni *post-hoc* test or Wilcox test, and p < 0.05 was considered to indicate statistical significance.

10. Clinical study

To assess the clinical feasibility of TLB in lung cancer patients, we launched a prospective study for NSCLC patients undergoing definitive RT. The first protocol (IRB 2017-09-120) included patients with stage I-III NSCLC according to the 8th American Joint Committee on Cancer staging manual and pathologic confirmation who were inoperable because of their medical condition. They were recommended to receive definitive RT, and dose-fractionations were determined based on the tumor size, location, and stage. Approximately 10 mL of whole blood sample was obtained at simulation for RT planning. During RT, blood samples were drawn after 1, 2, and 3 days and 1 week, followed by weekly sampling. Posttreatment samples were drawn at 1 month, followed by 3-month intervals for 2 years with chest computed tomography. The second protocol (IRB 2018-05-155) included clinically diagnosed lung cancer patients who failed to have a pathologic diagnosis or for whom diagnostic procedures were significantly risky. All other procedures were the same as in the first protocol.
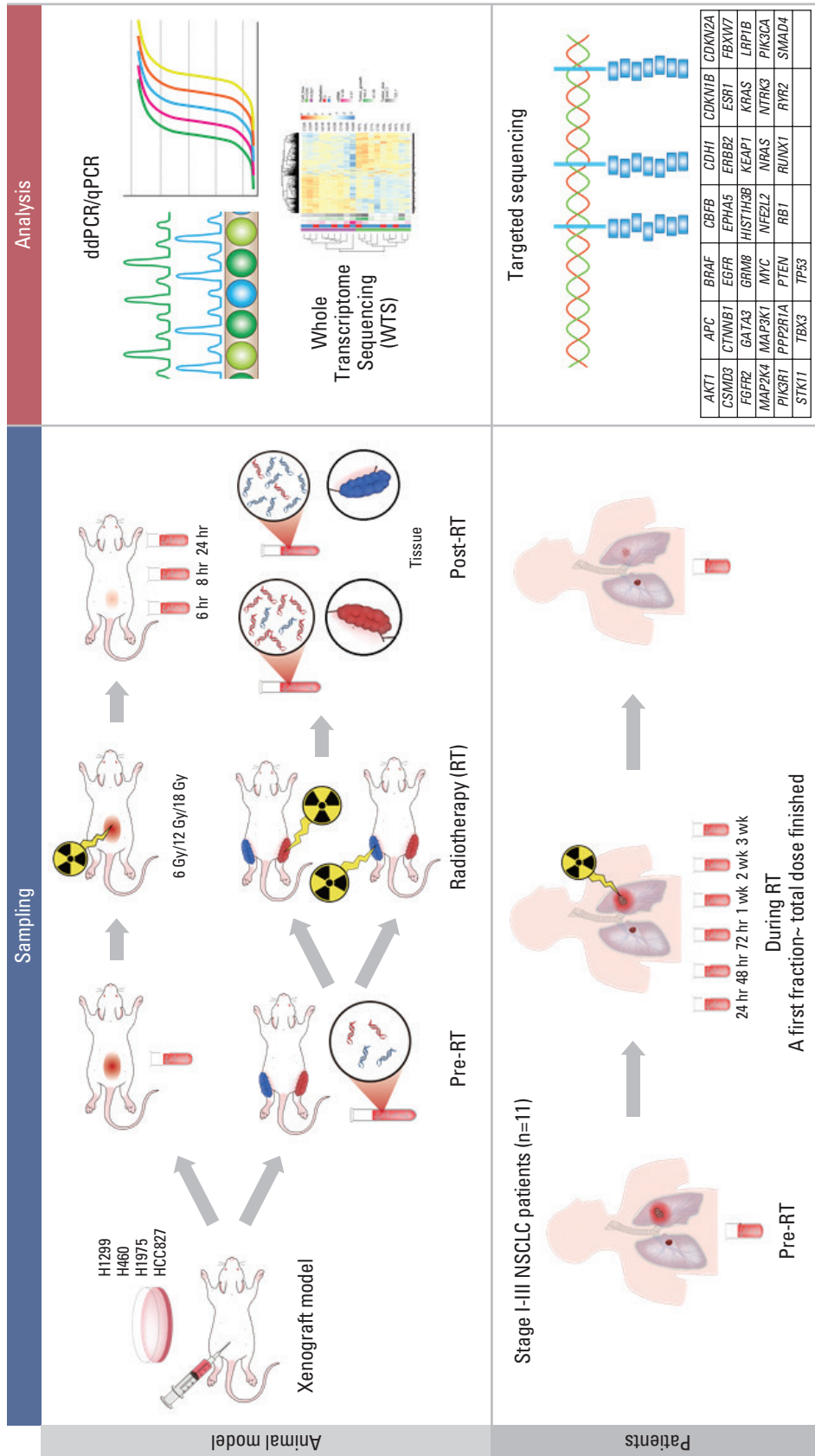
Fig. 1. Schematic view of the study design. In xenograft mouse model using human lung cancer lines; H460, H1299 (ras-mutant), H1975 and HCC827 (epidermal growth factor receptor [*EGFR*]-mutant), we estimated the effect of irradiation on circulating (cell-free) tumor DNA (ctDNA) level using human long interspersed nuclear element-1 quantitative polymerase chain reaction (qPCR) and mutation-specific droplet digital polymerase chain reaction (ddPCR). Irradiation of 6, 12, and 18 Gy was delivered on the tumor-bearing leg using 6-MV photon beams. Two-tumor xenograft model was developed inoculating H1299 and HCC827 to different legs. Then, prospective study for patients undergoing definitive radiotherapy (RT) with or without histologic diagnosis were launched, where targeted deep sequencing was performed to analyze ctDNA. NSCLC, non–small cell lung cancer.
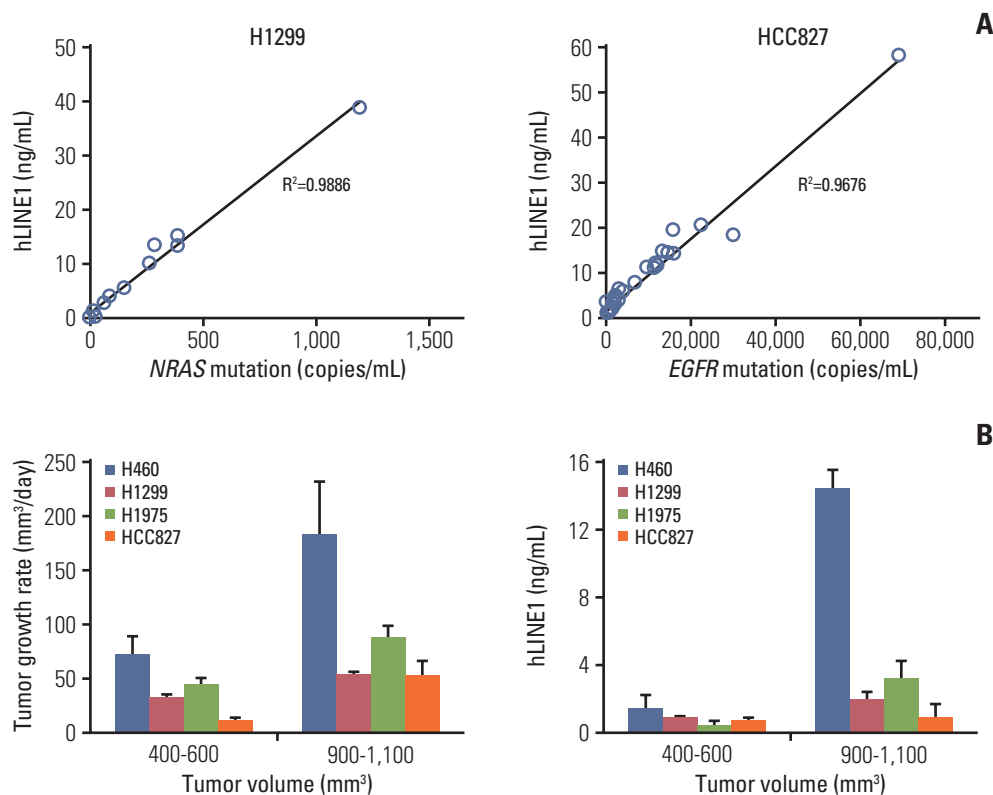
Fig. 2. Circulating human long interspersed nuclear element-1 (hLINE-1) DNA and tumor growth of various tumor models. (A) The concentration of plasma hLINE-1 correlated with the NRAS proto-oncogene, GTPase (*NRAS*) Q61K mutation in the H1299 xenograft model and the epidermal growth factor receptor (*EGFR*) E746-A750del mutation in the HCC827 xenograft model. (B) The tumor growth rate and concentration of plasma hLINE1 according to tumor volumes. Data represent means±standard error of mean (n=5).

Results

1. Assessment of circulating DNA from lung cancer xenograft model

First, we examined if RT is an adequate modality to promote cfDNA release from a targeted tumor tissue using mouse xenograft model as schemed in Fig. 1. Due to the small amounts of plasma DNA obtained from mouse xenograft models, we took advantage of the LINE-1, a repetitive sequence in the human genome. Because ~100,000 of these elements exist in the human genome and a subset of these copies can be distinguished from mouse orthologues, a quantitative real-time PCR method measuring human LINE-1 (hLINE-1) was successfully implemented to quantify ctDNA (i.e., human DNA) in small volumes of plasma samples from mouse xenograft models in a previous study [11]. As an alternative way to quantify ctDNA, we performed a droplet digital PCR method to count DNA fragments carrying *NRAS*/*EGFR* mutations, because the hLINE-1 assay could be used to discriminate ctDNAs released from different clonality of tumors (or cancer cell lines) despite its high sensitivity

for human DNA. To validate these methods to each other, we assessed correlation between hLINE-1 and *NRAS*/*EGFR* mutation copy numbers. The concentration of plasma hLINE-1 in the tumor-bearing mice correlated well with the *NRAS* Q61K mutation of the H1299 xenograft model and the *EGFR* E746-A750del mutation of the HCC827 xenograft model (Fig. 2A), demonstrating that both methods reliably quantified ctDNA in our mouse models.

To determine the relationship between tumor burden and ctDNA in the xenograft mouse models, we established mouse subcutaneous tumor models using various NSCLC cell lines. The xenograft models showed significant differences in tumor growth according to the various NSCLC cell lines (S2 Fig.), but the tumor growth rate and plasma hLINE-1 levels increased significantly in all cell lines when the tumor volume went above 900 mm^3. Thus, the correlation between the tumor growth rate and the hLINE-1 level was consistent within each cell line and across the four cell lines used in this study (Fig. 2B).

ctDNA could be measured using the amount of hLINE-1 or variation in the injected cells at tumor volumes of more than

400 mm², confirming that ctDNA reflects the tumor burden.

2. Increase in ctDNA by irradiation in lung cancer xenograft model

The hLINE-1 concentration increased significantly after irradiation in all animal models except the H1975 tumor model (Fig. 3A). Because ctDNA might be increased when tumor actively grew and more tumor cells died, we plotted the hLINE-1 concentration against the tumor growth rate to negate the possibility that the elevated hLINE-1 level in the irradiated mice (compared to that in the controls) was simply caused by a difference in the tumor growth rate. As shown in S3 Fig., the data showed that irradiation increased the hLINE-1 independently of tumor growth rate in H460, H1299, and HCC827. Among the three radiation-responsive cell lines, H1299 and HCC827 were chosen to further elucidate the ctDNA secretion caused by irradiation because they displayed similar tumor growth rates and carry different mutations. To select an optimal dose of irradiation and a time point to evaluate the response to irradiation, H1299 and HCC827 xenograft mice were irradiated with three different doses (6, 12, and 18 Gy) and sacrificed at three different time points after irradiation (6, 18, and 24 hours). The level of ctDNA was elevated upon irradiation at all tested doses. The elevation of the ctDNA level was consistently maintained from 6 hours to 24 hours, as observed in both the H1299 and HCC827 xenograft models (Fig. 3B). On the other hand, after irradiation, the concentration of cfDNA showed a small increase or no change in both models. Therefore, in further experiments, the mice were irradiated with 12 Gy and sacrificed 18 hours after irradiation to analyze ctDNA.

In addition to hLINE-1 quantitative PCR, we performed a ddPCR assay to quantify DNA fragments carrying tumor-specific mutations and thereby double check the elevated ctDNA levels upon irradiation. In H1299 tumor-bearing mice, the *NRAS* mutation increased after irradiation, which was more prominent in mice with larger tumors. The *EGFR* mutation also increased after irradiation in HCC827 tumor-bearing mice (Fig. 3C). Overall, we found that irradiation increased the level of ctDNA in the mouse lung-cancer xenograft models.

3. TLB using irradiation in double-xenograft mouse models

Based on the increased level of ctDNA after irradiation, we hypothesized that radiation aimed at a particular tumor region would locally facilitate ctDNA release from the irradiated region and thus enable TLB. TLB was anticipated not only to improve sensitivity of ctDNA but also to overcome tumor heterogeneity. To emulate intratumor genetic heterogeneity, we established two-tumor model mice bearing
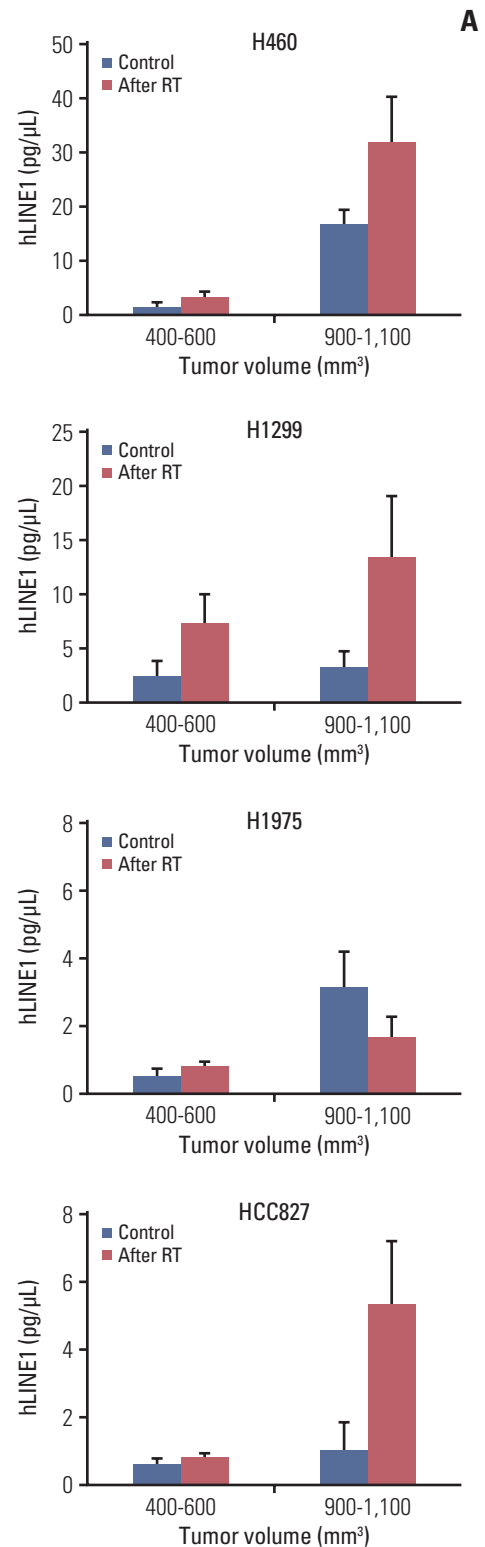
Fig. 3. Target-specific liquid biopsy using irradiation in xenograft mouse model. (A) The concentration of plasma human long interspersed nuclear element-1 (hLINE-1) in various tumor models before and after irradiation. *(Continued to the next page)*
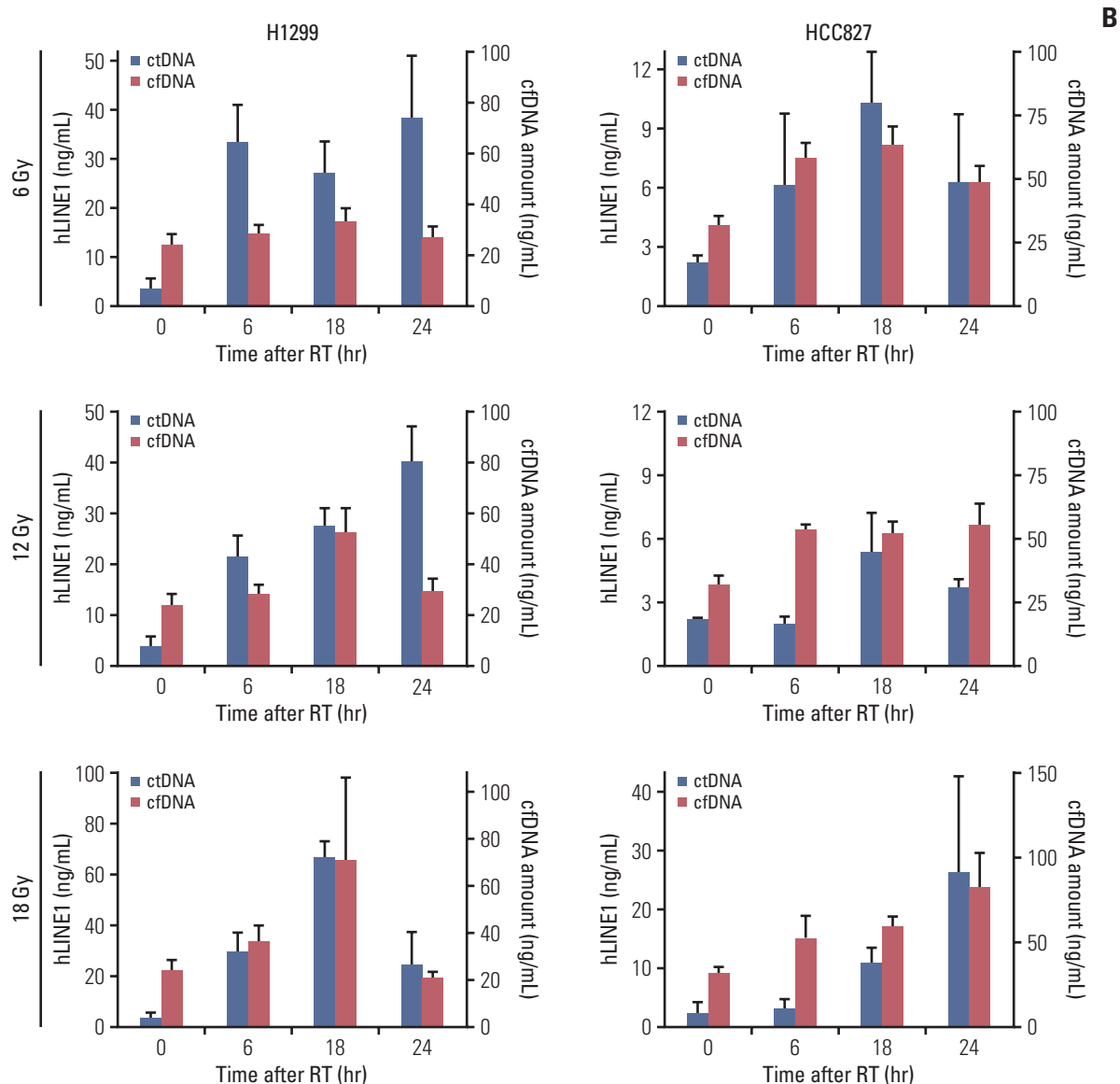
Fig. 3. *(Continued from the previous page)* (B) Three different doses (6, 12, and 18 Gy) and time points after irradiation (6, 18, and 24 hours) were examined. *(Continued to the next page)*

H1299 and HCC827 tumors, one in each hind leg.

To investigate the hypothesis, we irradiated one tumor site in two-tumor model mice. When irradiation was delivered to the H1299 tumor, *NRAS* Q61K was expected to increase, whereas the *EGFR* E746-A750del present in the HCC827 tumor was not expected to be affected. Similarly, the *EGFR* mutation, but not the *NRAS* Q61K mutation, was expected to increase when the HCC827 tumor was irradiated (Fig. 1). In the two-tumor model with H1299 and HCC827 tumors, an increase in the target-specific mutation was observed: *NRAS* Q61K copies increased only when the H1299 tumor was irradiated, and *EGFR* E746-A750del copies increased only upon

irradiation of the HCC827 tumor, suggesting preferential release of ctDNA from the irradiated tumors (Fig. 3D). These results confirm the feasibility of TLB in two-tumor mouse models.

4. Release of ctDNA from the tumor microenvironment

To investigate the mechanism by which the tumor microenvironment modulates releases of cell-free DNA from cancer cells into blood vessels, we performed transcriptome analysis of xenograft tumor tissues comprising tumor cells and infiltrated normal cells. We obtained both tumor tissues in the two-tumor mouse model and generated next-genera-
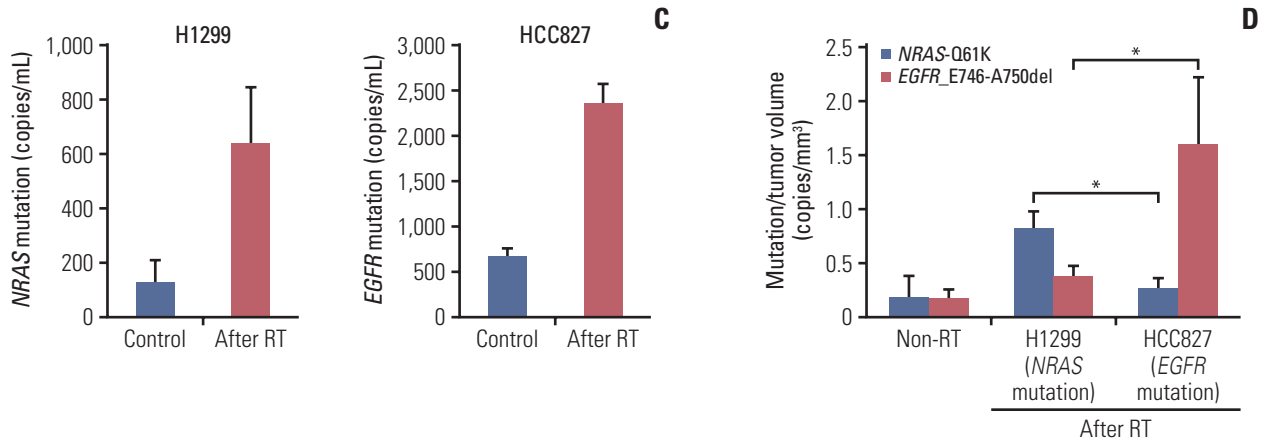
Fig. 3. *(Continued from the previous page)* (C) Tumor-specific mutations, *NRAS* mutation in the H1299 tumor model and *EGFR* mutation in the HCC827 tumor model, increased after irradiation in tumor-bearing mice. Data represent means±stasndard error of mean (SEM) (n=5). (D) When irradiating either the H1299 or HCC827-bearing leg in the two-tumor model, an increase in the target-specific mutation was observed. Data represent means±SEM (n=5). cfDNA, cell-free DNA; ctDNA, circulating (cell-free) tumor DNA; EGFR, epidermal growth factor receptor; NRAS, NRAS proto-oncogene, GTPase; RT, radiotherapy. *$p < 0.05$ compared with non-irradiation groups.

tion sequencing–based RNA sequencing (RNA-seq) data.

As a result, a mean of 19,144,381 human and 2,806,448 mouse reads were uniquely mapped to a concatenated human and mouse genome, indicating that 13.3% of transcripts were originated from host cells (Fig. 4A). In human transcripts, differentially expressed genes with or without irradiation did not show a common pattern in each sample and were clustered with the characteristics of the injected cell lines. The pattern was relatively weak, but the similar results in mouse transcripts was indicating that the two tumor cell lines interacted differently with host cells (Fig. 4B). When we listed host genes whose expression were significantly correlated with the level of ctDNA, most of the adjusted genes were functionally related to the cell cycle, apoptosis, metabolism, and DNA repair. In the absence of irradiation, transcriptional signatures were clustered by the injected cell line, and when they were exposed to radiation, interestingly, we confirmed that they clustered with genes related to ctDNA release (Fig. 4C).

Because recent studies showed that radiation, particularly high-dose, hypo-fractionated administration [12], stimulates the immune system, we investigated changes in the composition of the immune cells. To estimate the proportions of cell types contained in the tumor microenvironment, we deconvoluted the bulk RNA-seq data (the sum of the gene expression profiles of relevant cell types weighted by the proportion of each cell type) using cell type–specific gene expression references [10]. After irradiation, the cell fraction of macrophages and monocytes among the immune cells increased slightly, and natural killer (NK) cells decreased (Fig. 4D), which correlated with the amount of ctDNA (Fig.

4E). Immunohistochemical analysis of mouse tumors using markers of the mouse macrophage population also confirmed that macrophages increased after irradiation (Fig. 4F).

Taken together, our data indicated that the secretion of ctDNA following RT was not only caused directly by cancer cells but also indirectly related to changes in the cell composition of the tumor microenvironment.

5. Clinical feasibility of TLB in lung cancer patients

We launched a prospective study for patients undergoing definitive RT with or without a histologic diagnosis as schemed in Fig. 1. The first patient was a 78-year-old man with squamous cell carcinoma in the left upper lobe of his lung. The size of the primary tumor was 4.8 cm, and the clinical stage was T2bN1. He received definitive RT with a dose of 66 Gy in 22 fractions. Similar to our mouse tumor models, an elevation in the ctDNA level was observed 72 hours after the start of RT (Fig. 5A). The second patient was an 82-year-old man with a 1.9-cm tumor in the right lower lobe of his lung. Histologic diagnosis was judged to be difficult because of the tumor location, and he received hypo-fractionated RT with a dose of 64 Gy in 8 fractions. Despite the absence of a histologic diagnosis, several mutations were detected in the tumor DNA, and they increased after irradiation (Fig. 5B).

In total, we analyzed ctDNA in longitudinal blood samples from 11 patients (S4 Table). We observed a 2-fold increase in relative ctDNA levels 24-48 hours after the start of RT (Fig. 5C). Among the 11 patients, 10 (91%) showed temporary increase of the ctDNA within 72 hours after initiation of RT (Fig. 5D).
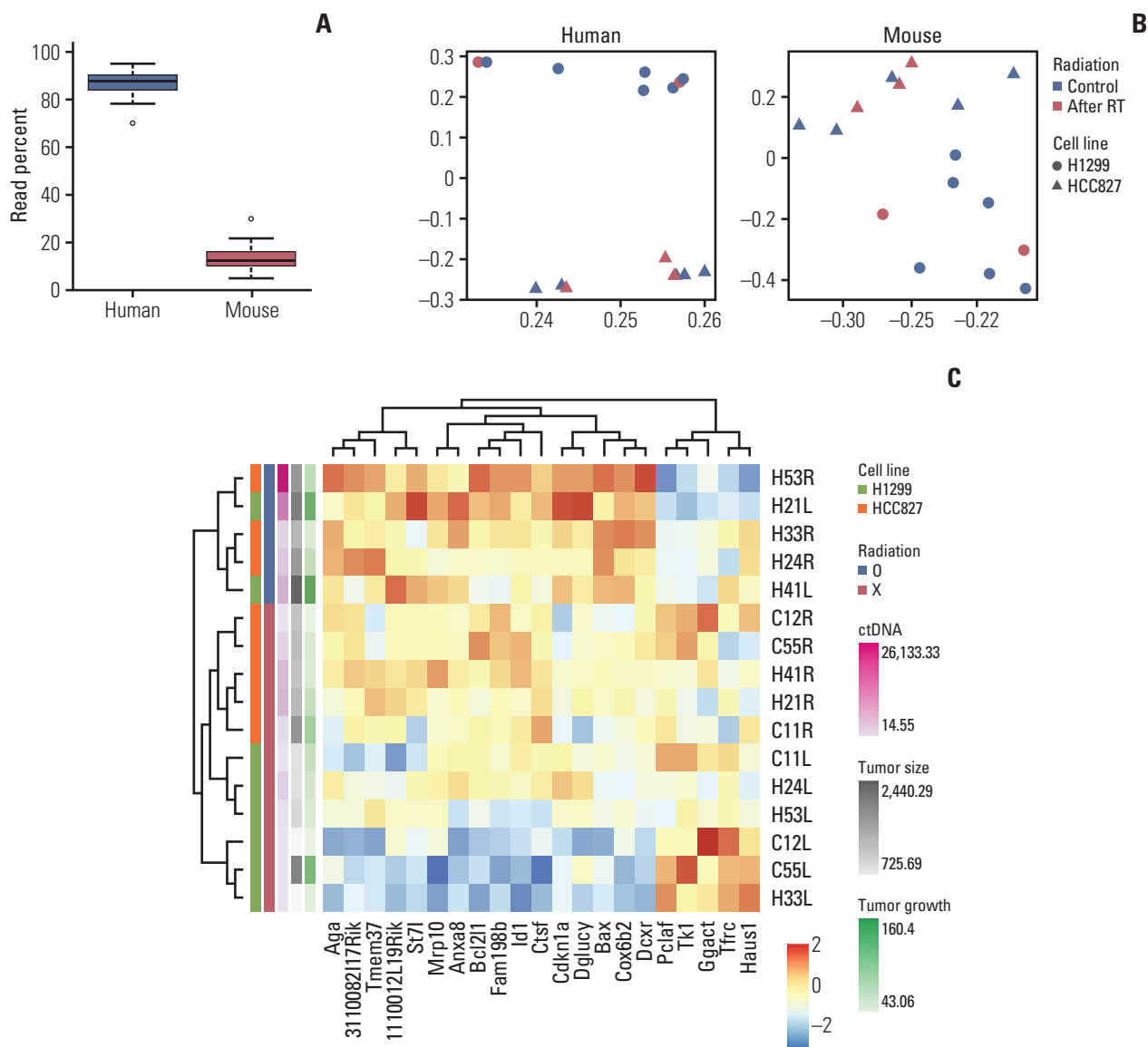
Fig. 4. Modulation of circulating (cell-free) tumor DNA (ctDNA) release by the tumor microenvironment. RNA sequencing (RNA-seq) transcriptome analysis of both tumor tissues in the two-tumor mouse model was performed. (A) Sequenced reads were mapped separately to the human and mouse genomes to delineate tumor (human) and host (mouse) gene expression. (B) Principal component analysis plots of the RNA-seq data show the characteristics of samples according to gene expression levels. Each dot indicates a sample. RT, radiotherapy. (C) Heat map of the transcriptome analysis for host genes correlated with ctDNA levels. Analysis of the varying cell-type proportions in the bulk data using a deconvolution method from the host gene. *(Continued to the next page)*

Discussion

During the past few decades, the emergence of precision medicine and personalized cancer treatment based on genetic analyses of tumor tissue has resulted in more specific treatment options. The shifting paradigm toward serially monitoring tumor molecular characteristics to more precisely guide therapy provides an opportunity for new diagnostic studies to determine the best way to acquire this information [13]. Liquid biopsy describes a noninvasive diagnostic approach that isolates and analyzes circulating tumor markers from peripheral blood. This technology could supplement existing clinical tools by improving the detection of recurrent cancer, monitoring treatment, and guiding therapy [14,15]. However, liquid biopsies for cancer diagnosis and treatment monitoring still have some challenging points for
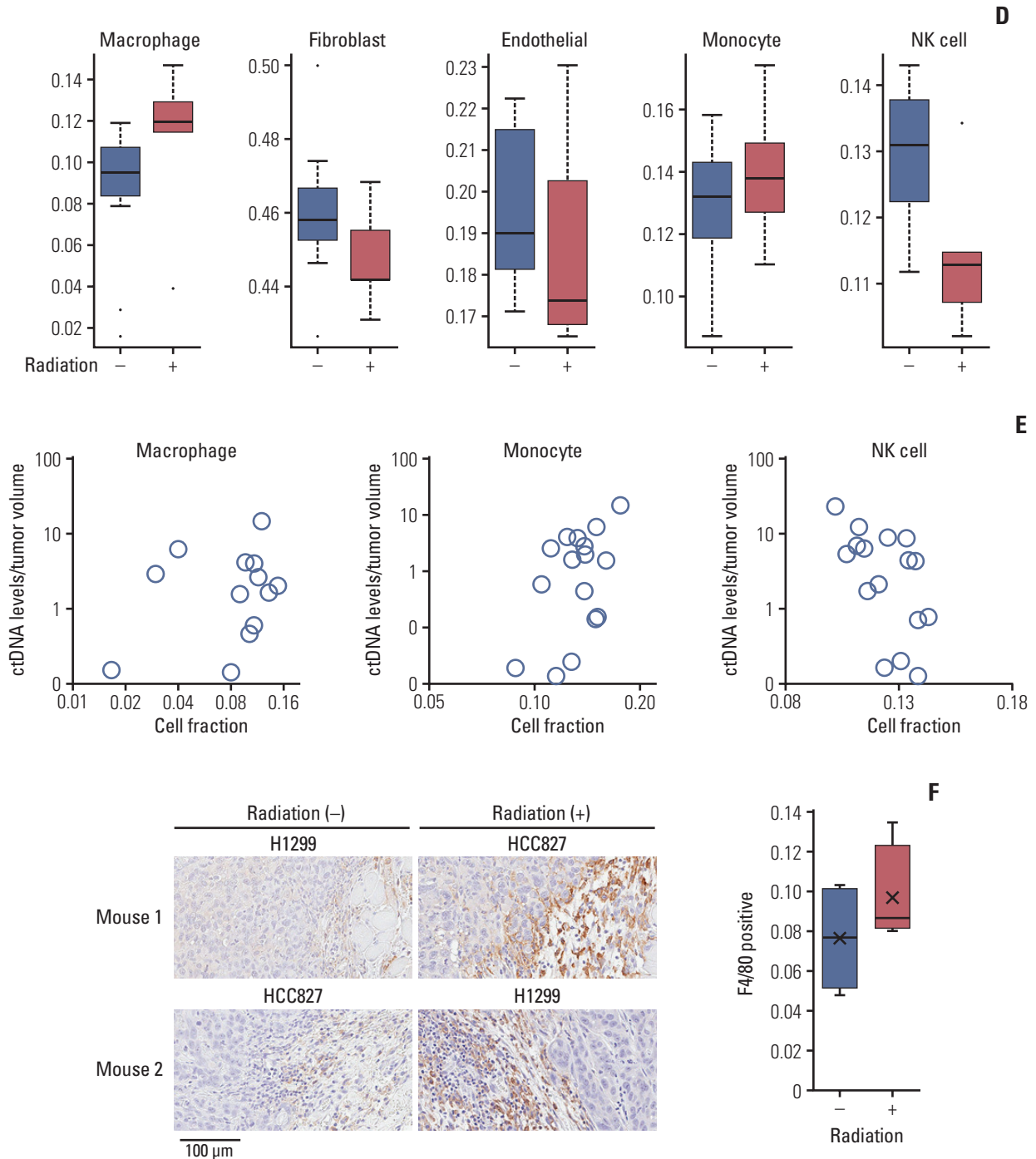
Fig. 4. *(Continued from the previous page)* (D) Changes in cell fractions after irradiation. (E) Correlation between the amount of ctDNA and the cell-type proportions by deconvolution in individual xenograft two-tumor model mice. NK, natural killer. (F) Immunohistochemical analysis of paraffin-embedded tumor tissues using F4/80. F4/80 is a cell surface protein and known marker of mouse macrophage populations.

clinical practice, and some questions need to be addressed further. One of the major clinical limitations is that the origin of biomarkers identified in a liquid biopsy cannot be identified. Another topic of interest is that the biomarkers are often present at or below the quantifiable limits. We sought to address those challenges by using irradiation to stimulate
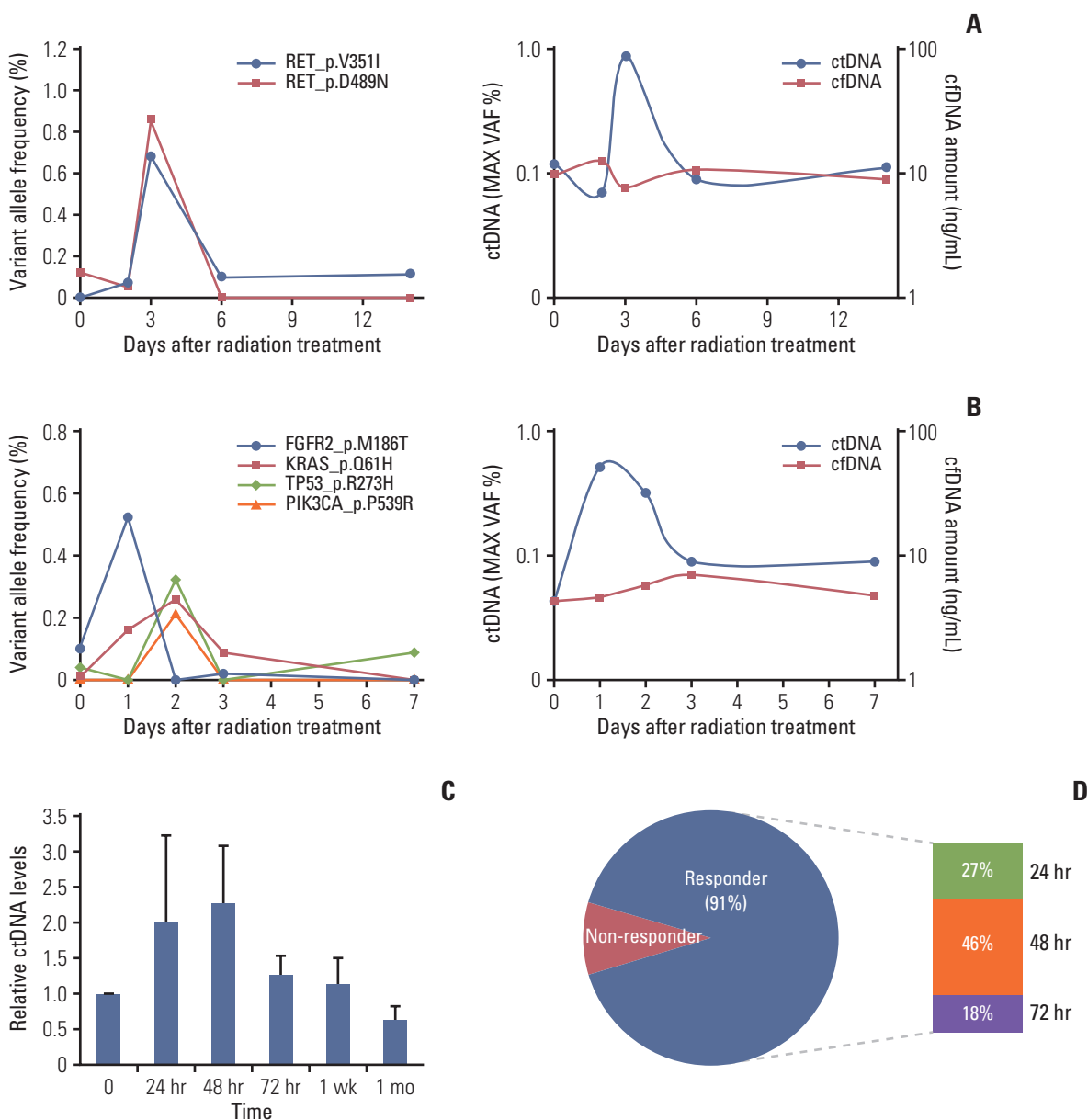
Fig. 5. Circulating (cell-free) tumor DNA (ctDNA) analysis after irradiation in patients with lung cancer. The ctDNA levels estimated by targeted deep sequencing are plotted on the left y-axis for patients with non–small cell lung cancer before and during radiotherapy. (A) Increase in ctDNA after radiotherapy for a patient with squamous cell carcinoma of the lung. (B) An increase was also observed in a patient with clinically diagnosed lung cancer without a histologic diagnosis. (C) Relative ctDNA levels of 11 patients with non–small cell lung cancer during radiotherapy (mean±standard error of mean). (D) Frequency of patients with increasing ctDNA levels over time after radiation therapy. Responders, patients with an increase in their ctDNA levels; non-responders, patients without an increase in their ctDNA levels. cfDNA, cell-free DNA.

the release of ctDNA from a precise anatomic location.

In this study, we demonstrated that RT temporarily amplifies the release ctDNA in lung cancer mouse models. We also demonstrated the feasibility of TLB in a double-xenograft mouse model. Preliminary results from our clinical study

also demonstrated a temporary increase in ctDNA following RT. In addition, monitoring of tumor response might be also feasible (Fig. 5). In this respect, accrual of more patients and longer follow-up is currently ongoing.

Although the plasma volumes from mouse xenograft

Table 1. Summary of previous studies on ctDNA during radiotherapy

Study (year)	Cancer type	No. of patients	Treatment	Implication
Chaudhuri et al. (2017) [23]	Lung cancer	40	RT/CRT Surgery	ctDNA analysis can identify posttreatment MRD
Moding et al. (2020) [27]	Lung cancer	65	CCRT±ICI	Consolidation ICI was beneficial in patients with MRD
Lv et al. (2019) [28]	Nasopharyngeal cancer	673	CRT	Persistent circulating EBV DNA was adverse prognostic factor
Chera et al. (2019) [29]	Oropharyngeal cancer	103	CRT	Rapid clearance profile of plasma HPV DNA predicts likelihood of disease control
Current study	Lung cancer	11	RT alone	Temporary increase of ctDNA within 72 hours after initiation of RT

CCRT, concurrent chemoradiation therapy; CRT, chemoradiotherapy; ctDNA, circulating (cell-free) tumor DNA; EBV, Epstein-Barr virus; HPV, human papillomavirus; ICI, immune check point inhibition; MRD, molecular residual disease; RT, radiotherapy.

models were small, we reliably used them to quantify ctDNA with both the hLINE-1 assay and digital PCR. At several doses, the concentration of ctDNA and cfDNA increased within 24 hours of irradiation except the H1975 tumor model. Different kinetics of cfDNA release might be affected by a complex interplay between apoptosis, necrosis, and senescence, as described by Rostami et al. [16]. Cellular senescence was increased following irradiation in NSCLC cells including H1975 and HCC827, and an inverse trend between senescence and cfDNA release was demonstrated. The time points of the current study were relatively early, while post-irradiation cfDNA release was little within 6-48 hours in the study by Rostami et al. [16]. But we observed an increase of ctDNA and cfDNA release within 24 hours including HCC827 xenograft model. Differences in irradiation dose (8 Gy vs. 6, 12, 18 Gy) and experimental setting (*in vitro* vs. *in vivo*) could affect these different results. In addition to cellular response, tumor microenvironment might be another key contributor of cfDNA release (Fig. 4).

Similar to patients with lung cancer, the total concentration of cfDNA in mice is known to increase as the disease progresses [17]. Although the concentration of hLINE-1 was higher in mice with larger tumors, the increase in the hLINE-1 concentration after RT on small tumors (Fig. 3A) suggests that RT could be used to enable a liquid biopsy for small tumors. A temporary increase in ctDNA after RT was also observed in the preliminary assessment of results from our clinical study (Fig. 5). Previously, early spike in ctDNA has been regarded to reflect cell death and treatment efficacy [18,19]. In terms of tumor detection and diagnosis, the current study might be helpful for patients with small tumors, in whom ctDNA might not otherwise be detected [3]. As shown in Fig. 5B, the increased ctDNA level in patients with clinically diagnosed lung cancer supports the diagnostic feasibility of liquid biopsy augmented by local irradiation.

In addition, target-specific amplification of ctDNA levels in the two-tumor mouse model suggests that the diagnostic value of liquid biopsy could be improved by using irradiation as a local stimulus. Although liquid biopsy itself cannot identify a specific site or represent intratumoral heterogeneity, local irradiation could make it target-specific. Therefore, we could apply this concept clinically to patients who need repeated liquid biopsies for tumor foci resistant to previous treatments. A future clinical study should assess the feasibility of TLB for patients with advanced disease who are receiving RT to treat a metastatic tumor.

Why did we use RT for ctDNA amplification? Other local stimulation methods might be used, such as high-intensity, focused ultrasound, but the lung environment is quite different from other solid organs. X-rays can be delivered anywhere precisely, and they are widely used to treat lung cancer. Clinically, lung cancer has various mutations that produce resistance to treatment, and serial liquid biopsy during systemic anticancer therapy is needed to identify response or progression [20]. Local RT has been increasingly applied in oligometastatic lung cancer patients [21,22], and TLB might benefit those patients by identifying relevant mutations, monitoring treatment response, and detecting MRD [3,6,23]. Recently, integrating cancer immunotherapy and RT has been widely investigated because of the immunomodulatory effect of RT [24]. As local radiation elicits immune responses, immune checkpoint inhibitors could enhance treatment response by inhibiting the radioresistant immune response [25]. While combinations of RT and immunotherapy have been widely tested in various lung cancer situations [26], a future study with a ctDNA analysis will monitor patients' responses to optimize combination of RT and immunotherapy [27].

Compared with previous studies on monitoring ctDNA

during RT or chemoradiotherapy, the current study has some limitations (Table 1) [23,27-29]. First, we only included 11 patients in clinical study, and long-term follow-up with monitoring treatment response was not included. Although the prognostic implication of ctDNA monitoring could not available in the current study, the preliminary object of the clinical study was to demonstrate temporally increase of ctDNA after RT (Fig. 5). Then, accrual of more patients and longer follow-up will address this limitation. Second, we included patients with RT alone, and only irradiation was applied to mouse model, too. Therefore, the results of the current study may be only useful for patients receiving RT. In clinical study, we aimed to observe the effect of RT itself, excluding the effects of other treatment such as concurrent chemotherapy. Including patients receiving treatment other than RT alone will be considered in future study. As application of local RT has been increased in patients with oligometastasis or oligoprogression of lung cancer, the results of the current study may be extended to patients receiving RT as a part of systemic treatment in these patients. The novel finding of the current study, targe-specific amplification of ctDNA levels in double-xenograft model which have different genotype, should be confirmed in future clinical study for patients with advanced disease who are receiving RT to metastasis tumor.

When we analyzed bulk RNA-seq data, the mouse gene expression profiles differed significantly between cell lines. This observation raised the possibility that ctDNA levels were partly influenced by specific interactions with the host system. Because radiation not only induces the death of tumor cells but also modulates the tumor microenvironment, the increase in ctDNA after irradiation might be related to changes in immune cell proportions or activities. The results of our bulk RNA-seq deconvolution analysis are consistent with the previous observation that irradiation modulates immune cells, such as macrophages and NK cell proportions [30-32]. Moreover, macrophages, which routinely phagocytose or scavenge dying cells from necrosis or apoptosis, have been suggested as a critical determinant of ctDNA level. In an *in vitro* cell co-culture study, the generation of cfDNA from dead and dying cells was reported to increase dramatically in the presence of macrophages [33]. Thus, we hypothesize that macrophages are recruited into tumor tissues upon irradiation and subsequently contribute to the release of ctDNA in the xenograft models.

In conclusion, we used irradiation and high-throughput techniques to temporarily amplify ctDNA release in both animal models and lung cancer patients to decipher the heterogeneity and distinct molecular signatures of a specific anatomical tumor site. TLB could have clinical utility for diagnosis and identifying relevant mutations in tumor foci resistant to previous treatments, and allow for serial liquid biopsies to monitor treatment response and to detect MRD during lung cancer treatment.

Electronic Supplementary Material

Supplementary materials are available at Cancer Research and Treatment website (https://www.e-crt.org).

Author Contributions

Conceived and designed the analysis: Noh JM, Lee HY, Choi C, Pyo H, Park WY.
Collected the data: Ahn WG, Park JH.
Contributed data or analysis tools: Kim YJ, Ahn WG, Lee T, Park D.
Performed the analysis: Kim YJ, Lee T.
Wrote the paper: Noh JM, Kim YJ, Park D.
Funding acquisition: Lee HY.
Study supervision: Pyo H, Park WY.
Technical support: Park D.

Conflicts of Interest

Conflict of interest relevant to this article was not reported.

References

1. Zheng D, Ye X, Zhang MZ, Sun Y, Wang JY, Ni J, et al. Plasma EGFR T790M ctDNA status is associated with clinical outcome in advanced NSCLC patients with acquired EGFR-TKI resistance. Sci Rep. 2016;6:20913.
2. Moding EJ, Diehn M, Wakelee HA. Circulating tumor DNA testing in advanced non-small cell lung cancer. Lung Cancer.

2018;119:42-7.

3. Newman AM, Bratman SV, To J, Wynne JF, Eclov NC, Modlin LA, et al. An ultrasensitive method for quantitating circulating tumor DNA with broad patient coverage. Nat Med. 2014;20:548-54.

4. Kato K, Uchida J, Kukita Y, Kumagai T, Nishino K, Inoue T, et al. Numerical indices based on circulating tumor DNA for the evaluation of therapeutic response and disease progression in lung cancer patients. Sci Rep. 2016;6:29093.

5. De Michino S, Aparnathi M, Rostami A, Lok BH, Bratman SV. The utility of liquid biopsies in radiation oncology. Int J Radiat Oncol Biol Phys. 2020;107:873-86.

6. Rostami A, Bratman SV. Utilizing circulating tumour DNA in radiation oncology. Radiother Oncol. 2017;124:357-64.

7. Baumann M, Krause M, Overgaard J, Debus J, Bentzen SM, Daartz J, et al. Radiation oncology in the era of precision medicine. Nat Rev Cancer. 2016;16:234-49.

8. Chaudhuri AA, Binkley MS, Osmundson EC, Alizadeh AA, Diehn M. Predicting radiotherapy responses and treatment outcomes through analysis of circulating tumor DNA. Semin Radiat Oncol. 2015;25:305-12.

9. Shin SH, Kim YJ, Lee D, Cho D, Ko YH, Cho J, et al. Analysis of circulating tumor DNA by targeted ultra-deep sequencing across various non-Hodgkin lymphoma subtypes. Leuk Lymphoma. 2019;60:2237-46.

10. Wang X, Park J, Susztak K, Zhang NR, Li M. Bulk tissue cell type deconvolution with multi-subject single-cell expression reference. Nat Commun. 2019;10:380.

11. Rago C, Huso DL, Diehl F, Karim B, Liu G, Papadopoulos N, et al. Serial assessment of human tumor burdens in mice by the analysis of circulating DNA. Cancer Res. 2007;67:9364-70.

12. Arnold KM, Flynn NJ, Raben A, Romak L, Yu Y, Dicker AP, et al. The impact of radiation on the tumor microenvironment: effect of dose and fractionation schedules. Cancer Growth Metastasis. 2018;11:1179064418761639.

13. Underwood JJ, Quadri RS, Kalva SP, Shah H, Sanjeevaiah AR, Beg MS, et al. Liquid biopsy for cancer: review and implications for the radiologist. Radiology. 2020;294:5-17.

14. Abbosh C, Birkbak NJ, Swanton C. Early stage NSCLC: challenges to implementing ctDNA-based screening and MRD detection. Nat Rev Clin Oncol. 2018;15:577-86.

15. Corcoran RB, Chabner BA. Application of cell-free DNA analysis to cancer treatment. N Engl J Med. 2018;379:1754-65.

16. Rostami A, Lambie M, Yu CW, Stambolic V, Waldron JN, Bratman SV. Senescence, necrosis, and apoptosis govern circulating cell-free DNA release kinetics. Cell Rep. 2020;31:107830.

17. Rakhit CP, Trigg RM, Le Quesne J, Kelly M, Shaw JA, Pritchard C, et al. Early detection of pre-malignant lesions in a KRAS(G12D)-driven mouse lung cancer model by monitoring circulating free DNA. Dis Model Mech. 2019;12:dmm036863.

18. Walls GM, McConnell L, McAleese J, Murray P, Lynch TB, Savage K, et al. Early circulating tumour DNA kinetics measured by ultra-deep next-generation sequencing during radical radiotherapy for non-small cell lung cancer: a feasibility study. Radiat Oncol. 2020;15:132.

19. Kato K, Uchida J, Kukita Y, Kumagai T, Nishino K, Inoue T, et al. Transient appearance of circulating tumor DNA associated with de novo treatment. Sci Rep. 2016;6:38639.

20. Wan JC, Massie C, Garcia-Corbacho J, Mouliere F, Brenton JD, Caldas C, et al. Liquid biopsies come of age: towards implementation of circulating tumour DNA. Nat Rev Cancer. 2017;17:223-38.

21. Gomez DR, Tang C, Zhang J, Blumenschein GR Jr, Hernandez M, Lee JJ, et al. Local consolidative therapy vs. maintenance therapy or observation for patients with oligometastatic non-small-cell lung cancer: long-term results of a multi-institutional, phase II, randomized study. J Clin Oncol. 2019;37:1558-65.

22. Iyengar P, Wardak Z, Gerber DE, Tumati V, Ahn C, Hughes RS, et al. Consolidative radiotherapy for limited metastatic non-small-cell lung cancer: a phase 2 randomized clinical trial. JAMA Oncol. 2018;4:e173501.

23. Chaudhuri AA, Chabon JJ, Lovejoy AF, Newman AM, Stehr H, Azad TD, et al. Early detection of molecular residual disease in localized lung cancer by circulating tumor DNA profiling. Cancer Discov. 2017;7:1394-403.

24. Daly ME, Monjazeb AM, Kelly K. Clinical trials integrating immunotherapy and radiation for non-small-cell lung cancer. J Thorac Oncol. 2015;10:1685-93.

25. Dolgin E. News feature: radiation redux. Proc Natl Acad Sci U S A. 2017;114:6416-20.

26. Hendriks LE, Menis J, De Ruysscher DK, Reck M. Combination of immunotherapy and radiotherapy: the next magic step in the management of lung cancer? J Thorac Oncol. 2020;15:166-9.

27. Moding EJ, Liu Y, Nabet BY, Chabon JJ, Chaudhuri AA, Hui AB, et al. Circulating tumor DNA dynamics predict benefit from consolidation immunotherapy in locally advanced non-small-cell lung cancer. Nat Cancer. 2020;1:176-83.

28. Lv J, Chen Y, Zhou G, Qi Z, Tan KR, Wang H, et al. Liquid biopsy tracking during sequential chemo-radiotherapy identifies distinct prognostic phenotypes in nasopharyngeal carcinoma. Nat Commun. 2019;10:3941.

29. Chera BS, Kumar S, Beaty BT, Marron D, Jefferys S, Green R, et al. Rapid clearance profile of plasma circulating tumor HPV type 16 DNA during chemoradiotherapy correlates with disease control in HPV-associated oropharyngeal cancer. Clin Cancer Res. 2019;25:4682-90.

30. Hietanen T, Pitkanen M, Kapanen M, Kellokumpu-Lehtinen PL. Effects of single and fractionated irradiation on natural killer cell populations: radiobiological characteristics of viability and cytotoxicity in vitro. Anticancer Res. 2015;35:5193-200.

31. Wu Q, Allouch A, Martins I, Modjtahedi N, Deutsch E, Perfettini JL. Macrophage biology plays a central role during ionizing radiation-elicited tumor response. Biomed J. 2017;40:200-11.

32. Shi X, Shiao SL. The role of macrophage phenotype in regulating the response to radiation therapy. Transl Res. 2018;191:64-80.

33. Choi JJ, Reich CF 3rd, Pisetsky DS. The role of macrophages in the in vitro generation of extracellular DNA from apoptotic and necrotic cells. Immunology. 2005;115:55-62.